Potential Energy Surface Crossings and the Mechanistic Spectrum for Intramolecular Electron Transfer in Organic Radical Cations

Lluís Blancafort,[†] Franck Jolibois,[†,§] Massimo Olivucci,[‡] and Michael A. Robb*[,†]

Contribution from the Department of Chemistry, King's College London, Strand, London WC2R 2LS, UK, and Dipartimento di Chimica, Università degli Studi di Siena, Via Aldo Moro, I-53100 Siena, Italy

Received September 12, 2000. Revised Manuscript Received October 26, 2000

Abstract: The structure of the potential energy surface for the intramolecular electron transfer (IET) of four different model radical cations has been determined by using reaction path mapping and conical intersection optimization at the ab initio CASSCF level of theory. We show that, remarkably, the calculated paths reside in regions of the ground-state energy surface whose structure can be understood in terms of the position and properties of a surface crossing between the ground and the first excited state of the reactant. Thus, in the norbornadiene radical cation and in an analogue compound formed by two cyclopentene units linked by a norbornyl bridge, IET proceeds along direct-overlap and super-exchange concerted paths, respectively, that are located far from a sloped conical intersection point and in a region where the excited-state and ground-state surfaces are well separated. A second potential energy surface structure has been documented for 1,2-diamino ethane radical cation and features two parallel concerted (direct) and stepwise (chemical) paths. In this case a peaked conical intersection is located between the two paths. Finally, a third type of energy surface is documented for the bismethyleneadamantane radical cation and occurs when there is, effectively, a seam of intersection points (not a conical intersection) which separates the reactant and product regions. Since the reaction path cannot avoid the intersection, IET can only occur nonadiabatically. These IET paths indicate that quite different IET mechanisms may operate in radical cations, revealing an unexpectedly enriched and flexible mechanistic spectrum. We show that the origin of each path can be analyzed and understood in terms of the one-dimensional Marcus−Hush model.

Introduction

The use of the computer to map the potential energy surface of thermally activated reactions has now become a standard practice in many chemical laboratories. Usually, one locates and characterizes the lowest-energy reaction path for the chemical reaction under investigation. Less frequently, the search is extended to parallel or alternative reaction paths which lie at higher energy but may be of interest when a particular substitution pattern is present in the reactant, or when the reaction occurs in an environment different from the gas phase. The set of all of the computed paths provides a direct and unambiguous way for determining the mechanistic spectrum of a specific chemical process. In any case, only the structure of the valleys (i.e., the lower-energy regions) of the $3N - 6$ dimensional potential energy surface (where N is the number of atoms of the reacting system) are mapped, and any information on the structure of higher-energy regions is simply disregarded as chemically uninteresting.

Conical intersections usually occur at molecular structures far removed from thermal reaction paths but are important as basic mechanistic elements for photochemical reactions.[1] For bound polyatomic molecules, the points of conical intersection where the ground- and first excited-state potential energy surfaces cross lie usually at the highest-energy regions of the ground-state energy surface. The energy of these points is usually too high to be sampled during the reactive motion in the ground state, and therefore potential energy surface crossings are normally of no interest in the mechanistic spectrum of closed-shell molecules. However, we and others have recently provided evidence that for unstable intermediates such as radical cations, the energy difference between the first excited- and ground-state energy surface is significantly reduced.[2,3] Under these conditions, the search and characterization of conical intersections has been shown to be useful for the characterization of the mechanistic spectrum associated to reactions such as molecular rearrangements and intramolecular electron transfer (IET).

In the present paper we construct the IET mechanistic spectrum of four prototypical donor−linker−acceptor systems by mapping both the higher-energy (surface crossings) and the surrounding lower-energy (reaction paths) regions of their ground-state potential energy surface. From the point of view of the ground-state surface, a conical intersection (CI) may appear as a sharp energy maximum (a singularity) when the energy is plotted along the two molecular coordinates corresponding to the gradient difference (GD) and nonadiabatic

[†] King's College London.

[‡] University of Siena.

[§] Current address: Laboratoire de Physique Quantique, IRSAMC, Bat. 3R1 B4, 118 Route de Narbonne, 31062 TOULOUSE Cedex, France.

(1) For general discussions, see: (a) Robb, M. A.; Garavelli, M.; Olivucci, M.; Bernardi, F. In *Reviews in Computational Chemistry*; Lipkowitz, K. B., Boyd, D. B., Eds.; Wiley-VCH: New York, 2000; Vol. 15, pp 87−212. (b) Bernardi, F.; Olivucci, M.; Robb, M. A. *Chem. Soc. Rev.* **1996**, *25*, 321−328. (c) Klessinger, M.; Michl, J. *Excited States and Photochemistry of Organic Molecules*; VCH: New York, 1995; pp 183−184.

(2) (a) Blancafort, L.; Adam, W.; González, D.; Olivucci, M.; Vreven, T.; Robb, M. A. *J. Am. Chem. Soc.* **1999**, *121*, 10583−10590. (b) Fernández, E.; Blancafort, L.; Olivucci, M.; Robb, M. A. *J. Am. Chem. Soc.* **2000**, *122*, 7528−7533.

(3) Sastry, G. N.; Bally, T.; Hrouda, V.; Cársky, P. *J. Am. Chem. Soc.* **1998**, *120*, 9323−9334.

10.1021/ja003359w CCC: $20.00
Published on Web 01/03/2001

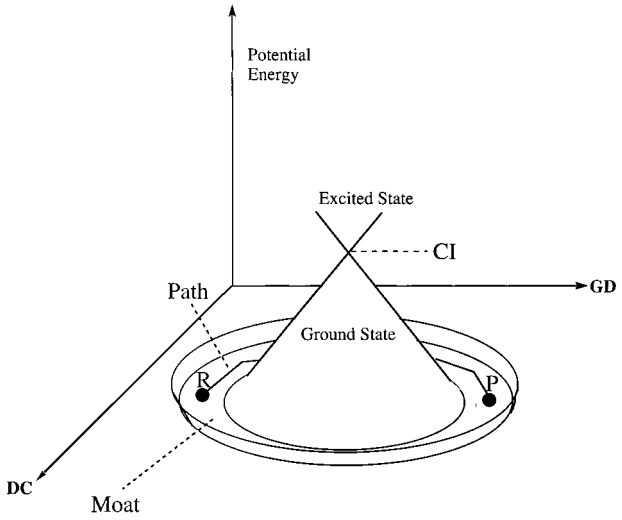

Figure 1. General, moat-shaped potential energy surface topology for the ground state in the vicinity of a peaked conical intersection.

coupling (DC) vectors (see Figure 1). These are the only two coordinates out of the $3N - 6$ geometric coordinates of the molecule that can split the ground-state/excited-state energy degeneracy at the CI.

The low-energy ground-state region surrounding such a maximum is the "moat" of the conical intersection since, in simple and well characterized (e.g., Jahn−Teller) systems such as H_3, it recalls the moat of a Mexican hat which contains three degenerate $H + H_2$ reaction paths (see Figure 1). In the radical cations under study, we will show that the mechanistically important reaction paths (indeed, the entire mechanistic spectrum) lie along one or more conical intersection moats. The molecular and electronic structure of a conical intersection correlates to that of the reactant (R), products (P), transition states, and intermediates located along the associated surrounding moat. In our recent work on the 1,2 rearrangement of housane radical cation, where a formal IET was embedded in the complex reactivity of the system,[2a] and in the IET of a bis(hydrazine) radical cation with a phenyl linker,[2b] we have demonstrated that, due to the reduced energy gap between the excited- and ground-state energy surface, conical intersection points either become structurally and energetically close to the moat IET paths or actually lie along an IET path. Obviously, in these cases the search and characterization of the different conical intersections and moats of the reacting system appears to be of basic importance.

Below, we present a general mechanistic spectrum of thermal IET derived by mapping of the conical intersections and moats along the potential energy surface of the norbornadiene radical cation (NRB), a NRB polycyclic analogue (PLN), the 1,2-diamino ethane radical cation (DAE), and the bismethyleneadamantane radical cation (BMA). These are all degenerate donor−linker−acceptor systems with an alkyl linker. We show that three different structures of the potential energy surface surrounding the CI of these species arise. These structures or topologies are classified according to the position and shape of the conical intersections and the associated moat and are illustrated in the diagrams of Figure 2. Notice that while these results are illustrated using a two-dimensional energy surface (which is approximately the cross section spanning the gradient difference and derivative coupling vectors), our calculations are carried out taking into account the full set of geometric coordinates of the molecules.

While the energetics and detailed molecular geometry of conical intersections (as well as that of the respective surrounding moats) will depend on the quantum chemical method used, the existence and topology (i.e., the shape of the surface) of such features can be establised at lower levels of theory. In the present paper we employ the ab initio CASSCF level of theory, which excludes the dynamic correlation energy. Therefore, the presented energetics cannot be used for predicting the dominant reaction path with accuracy or discussing the reaction kinetics. However, our main goal is to relate the calculated potential energy surface structure to the mechanistic IET spectrum.

We now briefly discuss the potential surface structures shown in Figure 2. Type 1 energy surface (Figure 2a) involves a potential energy surface characterized by a *single adiabatic reaction path*. This path can be associated with a so-called *sloped conical intersection* and a *sloped moat* (throughout the paper we use Ruedenberg's nomenclature[4] to classify the possible shape of conical intersections) or to a truly avoided crossing. Type 2 (Figure 2b) involves a *peaked conical intersection* with a *horizontal* moat. This surface has *two different adiabatic reaction paths* located on either side of the intersection. Finally, type 3 (Figure 2c) involves, effectively, *a "seam" of intersection* (not a single conical intersection point) separating the reactant and product regions. In this situation one finds a *single nonadiabatic path* with an unconventional "transition state" located at the lowest intersection point along the seam. These three types of surface structure may exist in different regions of the $3N - 6$ dimensional potential energy surface of a molecule, thus leading to a previously unsuspected rich and flexible mechanistic spectrum.

Our description of the potential energy surface does not provide kinetic information in the manner of the one-dimensional Marcus−Hush (MH) treatment,[5] by which IET is usually analyzed. However, it is much more general, since it provides different alternative IET paths that may or may not be consistent with the MH model. Thus, a second target in the present paper is to analyze and classify the "elements" of the computed reaction spectrum (i.e., the paths residing along the three types of potential energy surfaces given in Figure 2) in terms of MH-related cases (see Figure 3). In a donor−linker−acceptor molecule, the individual IET paths can occur by four different mechanisms: (i) by super-exchange[6] and (ii) by a nonadiabatic electron transfer (NAET) mechanism, (iii) by a "chemical" mechanism (CET), and (iv) by a direct-overlap mechanism. These mechanisms can, in turn, be related to a MH description. In the MH model, reactant and product are represented by two parabolas corresponding to two diabatic states (where the charge, i.e., the unpaired electron is localized on different parts of the molecule). The interaction between the two diabatic states at the transition-state geometry, controlled by the coupling term V, gives rise to the "real" adiabatic IET transition state. The coupling term V and the rate constant k of the IET are related to the optical absorption spectrum of the molecule. In mechanism (i), the term V is finite, due to indirect (through-bond) interaction of the donor and acceptor MOs via overlap with the linker MOs and to a small through-space contribution. Further, NAET (mechanism ii) occurs when the magnitude of the super-exchange or through-space couplings is very small. On the other hand, the standard MH scheme does not accommodate cases (iii) and (iv) quantitatively. In the direct-

(4) Atchity, G. J.; Xantheas, S. S.; Ruedenberg, K. *J. Chem. Phys.* **1991**, *95*, 1862−1876.

(5) (a) Newton, M. D. *Chem. Rev.* **1991**, *91*, 767−792. (c) Sutin, N. *Prog. Inorg. Chem.* **1983**, *30*, 441−498. (b) Marcus, R. A. *Annu. Rev. Phys. Chem.* **1964**, *15*, 155−196.

(6) (a) Cannon, R. D. In *Electron-Transfer Reactions*; Butterworth: London, 1980; pp 223−237. (b) Paddon-Row, M. N. *Acc. Chem. Res.* **1994**, *27*, 18−25.

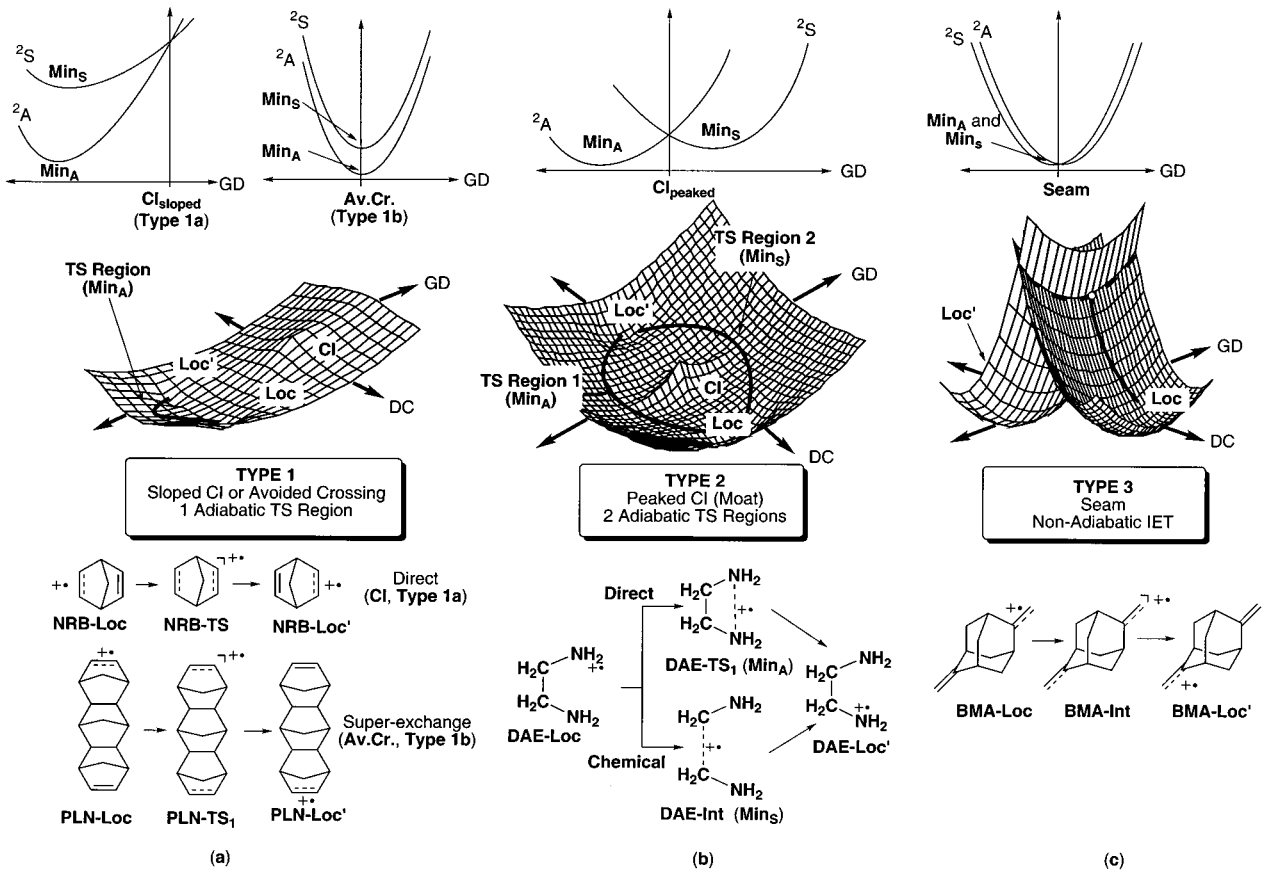

Figure 2. Potential energy surface topologies for intramolecular electron transfer in organic radical cations. The upper part shows a slice of the surface along the gradient difference coordinate (GD) at derivative coupling DC = 0. In the central part, only the lower part of the conical intersection (ground state of the potential energy surface) is shown in Figure 1a and b. In Figure 1a, only the sloped CI topology is shown.

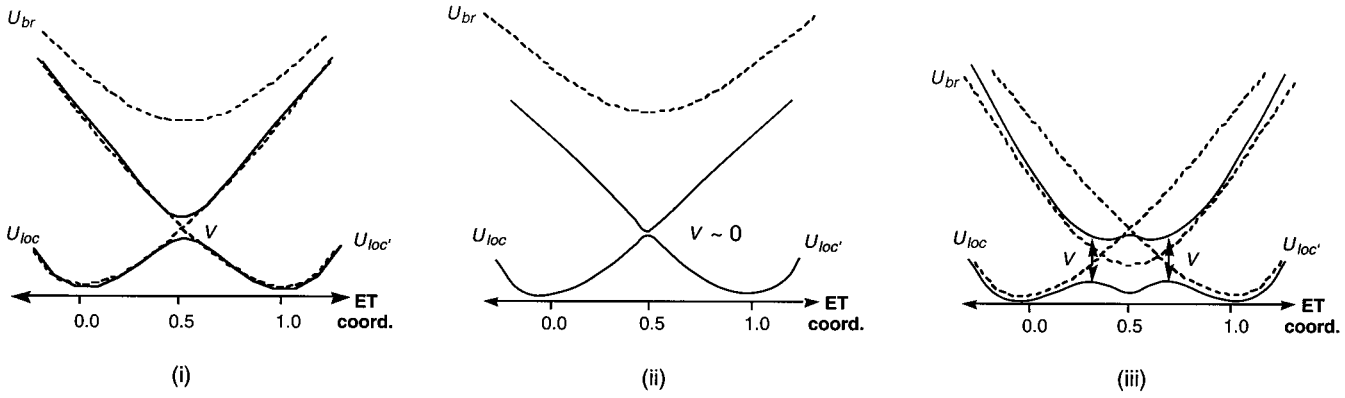

Figure 3. Marcus-Hush diagrams for the different IET mechanisms: (i) Super-exchange (small V). (ii) Nonadiabatic (NAET, $V \approx 0$). (iii) Chemical (U_{br} lowest diabatic state at transition state). Direct overlap (iv, not shown) is a variation of (i) with big V.

overlap case (iv), the term V due to through-space coupling is large, and the perturbation introduced in the MH model is too big for it to be valid. In contrast, for the CET mechanism (iii), the charge is actually located in the linker in the transition-state (TS) region, that is, the diabatic state of the bridge potential (U_{br}) is the lowest at the TS.[6a] Therefore, U_{br} should be included directly in the MH description, and such a three-state MH model has been recently proposed by Nelsen.[7]

Each mechanism (i−iv) can be assigned by examining (1) the calculated energy separation at the TS and (2) the charge residence on the linker. Thus, in (i) the energy separation at the TS is small and there is no point on the reaction path where the charge resides on the linker; while in (ii), there is also no charge residence on the linker, but, in addition, the energy separation at the TS is virtually zero. Moreover, in the adiabatic super-exchange path (i) the charge flow occurs gradually along the reaction coordinate, while in NAET (ii) the charge transfer, from a formal point of view, takes place "instantaneously" at the TS geometry. For the remaining cases, the energy separation at the TS is large, and there is charge residence on the linker in the CET (iii) but no charge residence on the linker for the direct case (iv).

(7) Nelsen, S. F.; Ismagilov, R. F.; Powell, D. R. *J. Am. Chem. Soc.* **1998**, *120*, 1924−1925.

On the basis of these criteria we now give a general overview where the results of our calculations are classified in terms of the topology (i.e., the shape) of the potential energy surface (types 1−3) and the mechanisms given above (i−iv). Type 1 topology (Figure 2a, one adiabatic TS) has been found for NRB and for the polycyclic analogue PLN (which have been studied as model compounds for IET both experimentally and theoretically[8]). In NRB, the adiabatic TS electronic structure arises from a donor−acceptor direct overlap (mechanism iv), while for PLN the super-exchange mechanism (i) applies. Type 2 potential energy surface has been previously documented for the 1,2 rearrangement of housane radical cation and IET in bis(hydrazine) radical cations with a phenyl linker.[2] In this paper this topology has been found for the DAE radical cation, where the two paths around the conical intersection correspond to a CET and a direct mechanism (cases (iii) and (iv), respectively). The CET path goes through an intermediate where the charge is localized on the carbon−carbon σ bond of the ethylene bridge. Type 3 surface structure, involving NAET through a seam of intersection (previously described for the crossing of the hydrazine-localized states of a model bis(hydrazine)[2b]), has been found in BMA (recently used as model compound for "symmetry-forbidden" IET dynamic calculations[9]). As in the bis(hydrazine) model, the seam topology for BMA arises because the super-exchange coupling between donor and acceptor is virtually zero, due to the perpendicular orientation of the charge-bearing groups (mechanism ii). Finally, for PLN, in addition to the super-exchange model, we have also located a CET mechanism (via an intermediate where the charge is localized in the rigid alkyl linker). This mechanism (iii) goes through a "conventional" TS, where the separation between the adiabatic states is estimated to be 10−20 kcal mol^{-1}.

Theoretical Considerations

The states which intersect in the model radical cations studied in this paper are characterized by the localization of the unpaired electron in one or the other of two possible singly occupied orbitals. At the TS region, for all of the cases we have studied thus far (with the exception of the chemical mechanism for PLN, which will be discussed later), the molecule is symmetric with respect to interchange of the donor−acceptor, and the charge-bearing orbitals are delocalized. There are two possible symmetries of the orbitals, symmetric or antisymmetric with respect to the symmetry operation that interchanges the donor−acceptor. For the sake of clarity, we will call these S and A orbitals, respectively. At the CI, the two crossing states are ^{2}S and ^{2}A, which are represented in the upper part of Figure 2. As mentioned above,[1,2,10] at the CI there are two degeneracy-lifting coordinates: the gradient difference and the derivative coupling. For a change of geometry along the derivative coupling coordinate, which must be nontotally symmetric, the S and A orbitals can mix, and the unpaired electron localizes. Accordingly, displacement from the CI along the derivative coupling leads to the two minima for the IET, where the electron is localized on donor or acceptor. For a change of geometry along the gradient difference, which must be totally symmetric, there are two minima, one for the ^{2}S state and one for the ^{2}A state, where the charge is delocalized. These minima are marked **Min$_S$** and **Min$_A$** in the top row of Figure 2. In the full space of coordinates, these symmetry-restricted minima **Min$_S$** and **Min$_A$** may be either reaction intermediates (thus yielding a stepwise IET process) or TS (thus yielding a concerted IET process). For a type 1 topology, one minimum may lie on the ground state, while the other is on the excited state. In this case, the two states may cross near the minima (type 1a, sloped intersection[4]) or at infinity (type 1b, truly avoided crossing). Alternatively, in the case of a peaked conical intersection (type 2, Figure 2b) both minima can lie on the ground state. In the special case of type 3 (Figure 2c), the two minima and the crossing point coincide, thus generating a seam of intersection. (A seam of intersection is a $(n-1)$-dimensional crossing between two potential energy surfaces, where n is the total number of degrees of freedom of the molecule, while a conical intersection is a $(n-2)$-dimensional crossing.)

While the MH description uses diabatic states, the states used in our work are the adiabatic states and the interaction V is already included everywhere. Thus, we are concerned always with *real* crossings. At a peaked CI, the degeneracy is lifted by two *nuclear* coordinates. One of these, the derivative coupling coordinate, corresponds, in the TS region, to the reaction coordinate in the MH model. However, the degeneracy of the two states at the CI is also lifted along a different nuclear displacement, the gradient difference, which is the additional coordinate of our two-dimensional model. In a peaked CI, this yields two different (symmetry-restricted) ground-state minima for the delocalized states. This situation, shown as type 2 (Figure 2b), has no simple counterpart in the MH description, where only a single reaction path is considered[5] which approximately coincides with the derivative coupling coordinate in our approach. Therefore, two separate MH diagrams would be necessary to describe the situation (one for each reaction path). For the topologies associated with type 1 or type 3, there is effectively only one reaction path, and there is closer relationship with MH theory. Thus, type 1 or 3 are charaterized by a finite or zero V in MH theory, respectively. In the case of a seam (type 3), the reaction path may be completely nonadiabatic. Further, if the crossing point for the sloped intersection (type 1) is close to the minimum, there may be large nonadiabatic effects. Thus, two geometrical coordinates rather than one are essential to describe the IET process in general.

Finally, we warn the reader of a conceptual and semantic problem. Since in our calculations we use delocalized, symmetry-adapted states at the conical intersection, the nuclear coordinate that leads from the crossing point to the localized minima is parallel to the direction of the derivative coupling vector computed at the CI. This vector is always nontotally symmetric, and as one moves away from the conical intersection point, the orbitals localize spontaneously. On the other hand, the coordinate which leads from the CI to the transition state(s) (**Min$_S$** and/or **Min$_A$**) of the IET is the gradient difference coordinate, which must be totally symmetric. However, since any linear combination of the degenerate wave functions is valid at the point of degeneracy, one could equally well choose the orbitals to be localized. In this case, the roles of the derivative coupling vector and the gradient difference vector are interchanged. Thus, in the localized orbital basis used in MH theory, even at the point of crossing, the IET reaction coordinate would be the gradient difference. The same happens at one of the crossings reported in this paper, the peaked CI found for the chemical mechanism in PLN (see below).

(8) (a) Jørgensen, F. S.; Paddon-Row, M. N.; Patney, H. K. *J. Chem. Soc., Chem. Commun.* **1983**, 573−575. (b) Balaji, V.; Ng, L.; Jordan, K. D.; Paddon-Row, M. N.; Patney, H. K. *J. Am. Chem. Soc.* **1987**, *109*, 6957−6969. (c) Paddon-Row, M. N.; Wong, S. S.; Jordan, K. W. *J. Am. Chem. Soc.* **1990**, *112*, 1710−1722. (d) Jones, G. A.; Carpenter, B. K.; Paddon-Row, M. N. *J. Am. Chem. Soc.* **1998**, *120*, 5499−5508.

(9) Jones, G. A.; Carpenter, B. K.; Paddon-Row, M. N. *J. Am. Chem. Soc.* **1999**, *121*, 11171−11178.

(10) Davidson, E. R. *J. Am. Chem. Soc.* **1977**, *99*, 397−402.

Table 1. Relative CASSCF/6-31G* Energies (in kcal mol^{-1})[a]

structure	symmetry	state	E_{rel}[b]	ΔE_{D1-D2}
NRB-Loc	C_s	$^2A'$	0.0	56.5
NRB-TS	C_{2v}	$^2B_2$	0.1	61.1
NRB-Exc	C_{2v}	$^2A_1$	19.6	16.4
NRB−CI	C_{2v}	$^2A_1/^2B_2$	38.2	0.0
PLN-Loc	C_s	$2A'$	0.0	12.9
PLN-TS$_1$	C_{2v}	$^2B_2$	0.6	6.8
PLN-Exc	C_{2v}	$^2A_1$	7.5[c]	7.2
PLN−CI	C_s	$2A'/2A'$	15.5[c]	0.0
PLN−Int$_1$	C_s	$2A'$	10.0	23.7
PLN−Int$_2$	C_1	2A	−1.1[d]	41.6
PLN-TS$_2$	C_s	$2A'$	11.0	11.7
PLN-TS$_3$	C_1	2A	10.0[d]	15.4
PLN-TS$_4$	C_s	$2A''$	10.2[e]	18.8
DAE-Loc	C_1	2A	0.0	*f*
DAE-Int	C_2	2A	5.9	*f*
DAE-TS$_1$	C_2	2B	7.8	*f*
DAE-TS$_2$	C_1	2A	7.2	*f*
DAE-CI	C_{2v}	$^2A_1/^2B_2$	35.2	0.0
DAE$_1$	C_s	$2A'$	5.6	*f*
DAE$_2$	C_{2v}	$^2B_2$	8.7	*f*
DAE$_3$	C_{2v}	$^2A_1$	9.8	*f*
BMA-Loc	C_{2v}	$^2B_1$	0.0	14.7
BMA-Int	D_2	$^2B_3$	3.24	0.47
BMA-CI	D_{2d}	2E	3.36	0.0

[a] Geometries optimized with the 6-31G* basis set for the NRB and DAE structures and with the 3-21G* basis set for the PLNO and BMA ones. See Tables S1−S3, Supporting Information, for the active spaces and the absolute energies. [b] Relative to the localized structures of each molecule except where noted. [c] Optimized 3-21G* value. [d] Relative to **PLNO−Int$_1$**. [e] Relative to **PLNO−Int$_2$**. [f] Not calculated; see text.

Computational Details

The CASSCF computations have been carried out with a development version of the Gaussian program.[11] A method for state-averaged frequency computations has been implemented in this code.[12] The relative energies of all structures are listed in Table 1. A complete documentation of the active space for all calculations is found in Tables S1−S3 of the Supporting Information.

In our CASSCF calculations for DAE, we used the 6-31G* basis set and an active space of 7 electrons in 6 orbitals: the two nitrogen nonbonding orbitals and the four orbitals corresponding to the two CN bonds of the molecule. In the optimizations and analytical frequency calculations, redundant orbitals (that is, orbitals with occupation numbers larger than 1.99 or smaller than 0.01) were removed from the active space. To compute the energetics for the direct path presented in Figure 2, single-point calculations using the "full" (7,6) active space were carried out on the optimized structures. For the structures with appreciable charge localization in the CC bond (**DAE-Int** and **DAE-TS$_2$**), the active space included the CC bond instead of the doubly occupied nitrogen orbital. To assess the energetics of the CET path, the energy of **DAE-Loc** was recomputed with this (7,7) active space. The possibility of spurious symmetry breaking was studied at a structure of C_{2v} geometry (corresponding to structure **DAE$_1$**). Use of a symmetry-broken wave function (localized nitrogen orbitals) gave virtually the same energy (0.002 kcal mol^{-1} higher) than the one obtained with symmetric orbitals. This confirms that there is no spurious symmetry breaking at the CASSCF(7,6)/6-31G* level.

For NRB, PLN, and BMA, the basic active space was 3 electrons in 4 orbitals (the 4 orbitals of the external double bonds). The NRB optimizations were carried out with the 6-31G* basis set. The optimizations of all other structures were carried out with the 3-21G* basis set, and the energy was recomputed with single-point 6-31G* calculations. For **NRB-Loc**, **NRB-TS** (Figure 4), **PLN-TS$_1$**, **BMA-Loc**, and **BMA-Int**, state-averaged orbitals were used during the optimizations and the analytical frequency calculations.[12] For **PLN-Loc** (Figure 5), the energy of the optimized structure was recalculated with state-averaged orbitals. This was due to the proximity of the two lowest states (see Table 1 for details) and prevented spurious symmetry breaking. The reaction coordinates shown in Figure 6 and Figure S1 (Supporting Information) were obtained by single-point calculations on geometries interpolated linearly between the corresponding minima and transition structures. In Figure 6, the occupations of the π bonds were obtained localizing the active space.

For the structures of the chemical path for PLN, the active space was enlarged, including the orbitals corresponding to the charge-bearing carbon−carbon σ bonds. State-averaged orbitals were also used for the optimization of **PLN-TS$_2$**. Due to the size of the problem, the structures of the chemical path for PLN were not characterized by frequency calculations. Instead, the TSs were optimized using numerical derivation along the IET coordinates (stretching of the involved carbon−carbon bonds). To compare the energies of all structures involved in the chemical path, it would be necessary to include all carbon−carbon σ bonds which carry charges in any of the structures. This would result in an (11,12) active space, which is too large. Instead, the energies for every step of the stepwise IET path shown in Scheme 1 were recomputed with single-point calculations. The single-point energies of structures **PLN−Int$_1$** and **PLN−Int$_2$**, which appear in two steps, were computed twice, each time with the active space adequate for the reaction step to be assessed. The (7,8) active spaces used in these single-point calculations are detailed in the Supporting Information section, Table S1. For the first step, the energies of the three structures **PLN-Loc**, **PLN-TS$_1$**, and **PLN−Int$_1$** were recomputed state averaging over the three lowest states.

In this work we have also considered the possibility of using alternative computational methods for our calculations, but found that none of them was useful for our problem. For DAE, QCISD/6-31G* calculations showed symmetry breaking at the C_{2v} geometry of **DAE$_1$**. Thus, by using a wave function of C_s symmetry (orbital localization at the nitrogens) with a C_{2v} geometry, the energy was spuriously lowered by 0.5 kcal mol^{-1}. As for B3LYP calculations, it is well-known that this method is inadequate for the calculation of small radical cations such as DAE, because it gives a wrong preference for charge-delocalized structures.[13] In fact, Carpenter and Paddon-Row report the same problem for PLN.[8d] For the latter system, we tried the viability of MP2/3-21G* calculations but found the same problem than for B3LYP.

Results and Discussion

In what follows we describe the potential energy surface topologies for the studied molecules. All topologies were characterized following the methodology described in our previous papers on radical cations,[2] which has been reviewed in the previous two subsections. In general, the CI of high symmetry was optimized first. Then, starting at the CI, following the gradient difference and derivative coupling coordinates, the relevant stationary points in the "moat" were optimized and characterized. The relative energies of all structures are presented in Table 1. Details of the geometries can be obtained from the Cartesian coordinates given in the Supporting Information.

Type 1 Topology: NRB and PLN. The potential energy surface of the radical cation of NRB is centered on a sloped CI of C_{2v} symmetry. The two crossing states (see Figure 4a) are the $^2B_2$ (electronic configuration $(a_1)^2(b_2)^1$) and the $^2A_1$ state (electronic configuration $(b_2)^2(a_1)^1$). Following the derivative coupling of b_2 symmetry (antisymmetric stretching of the double bonds), the charge localizes on one of the double bonds, and the localized minimum **NRB-Loc** is found. The minima of the two crossing states (i.e., the transition-state region for IET) were

(11) Frisch, M. J.; Trucks, G. W.; Schlegel, H. B.; Gill, P. M. W.; Johnson, B. G.; Robb, M. A.; Cheeseman, J. R.; Keith, T.; Petersson, G. A.; Montgomery, J. A.; Raghavachari, K.; Al-Laham, M. A.; Zakrzewski, V. G.; Ortiz, J. V.; Foresman, J. B.; Cioslowski, J.; Stefanov, B. B.; Nanayakkara, A.; Challacombe, M.; Peng, C. Y.; Ayala, P. Y.; Chen, W.; Wong, M. W.; Andres, J. L.; Replogle, E. S.; Gomperts, R.; Martin, R. L.; Fox, D. J.; Binkley, J. S.; Defrees, D. J.; Baker, J.; Stewart, J. P.; Head-Gordon, M.; Gonzalez, C.; and Pople, J. A. *Gaussian 98*;Gaussian, Inc.: Pittsburgh, PA, 1999.

(12) Vreven, T. Ph.D. Thesis, University of London, 1998.

(13) Bally, T.; Borden, W. T. *Rev. Comput. Chem.* **1998**, *13*, 1−97.

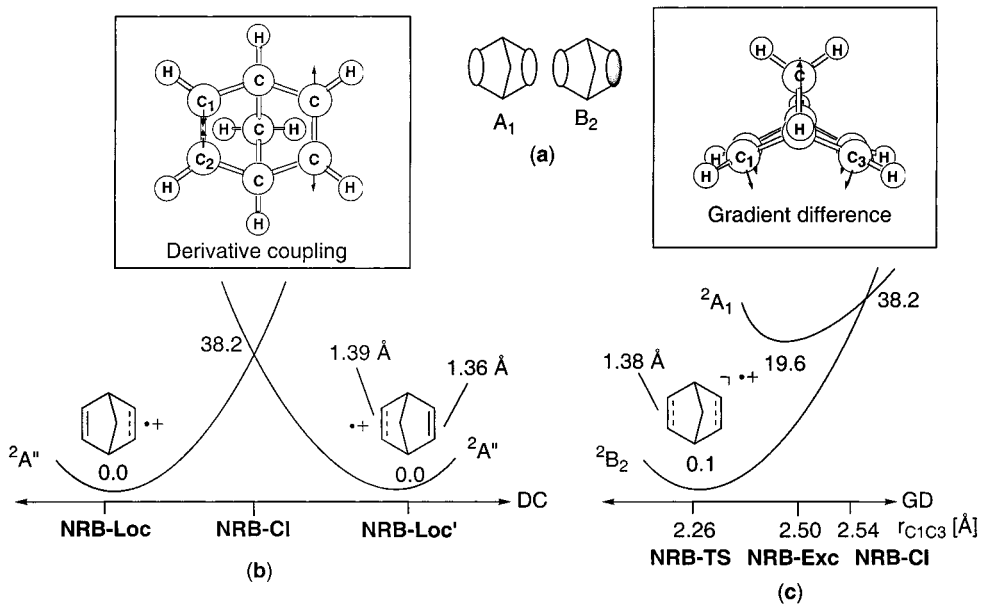

Figure 4. Branching of the NRB potential energy surface from the sloped CI along the derivative coupling (DC) and gradient difference (GD) coordinates (energies in kcal mol^{-1}).

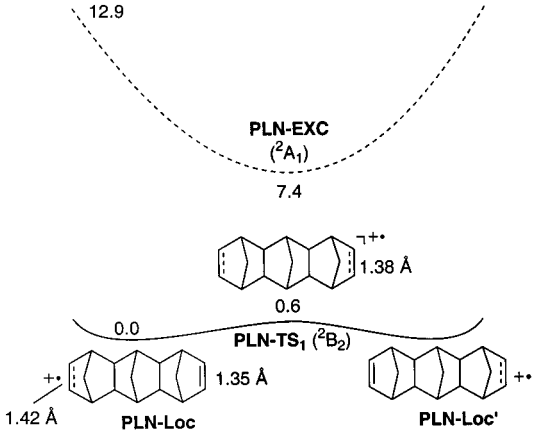

Figure 5. Intramolecular electron-transfer reaction coordinate for PLN (full line). The excited state is shown as a dashed line (energies in kcal mol^{-1}).

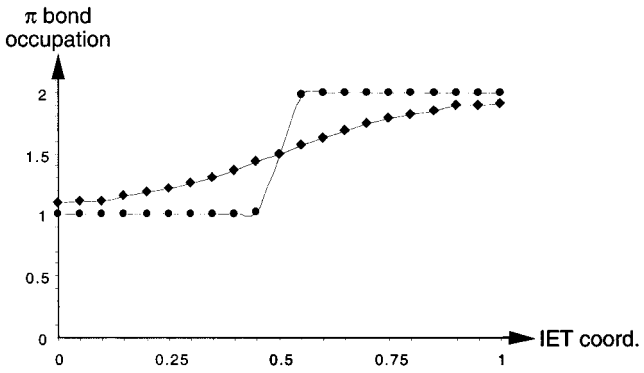

Figure 6. π bond occupation (only one bond shown for each compound) for PLNO (squares, gradual charge flow) and BMA (circles, instantaneous charge transfer at the TS) along the IET coordinate (see Computational Details).

found following the gradient difference coordinate (bending of the six-membered ring as shown in Figure 4) from the CI, in the *same* direction, both in the ground and excited-state energy surfaces. Thus, the $^2B_2$ minimum **NRB-TS** lies on the ground state of the potential energy surface, while the $^2A_1$ one, **NRB-Exc**, lies on the excited state. This gives rise to the type 1a topology of the surface. In the full space of coordinates, **NRB-TS** is the ground-state TS for the IET. Due to the sloped CI topology of the potential energy surface, there is only one TS for IET. The activation barrier is 0.1 kcal mol^{-1} at the CASSCF-(3,4)/6-31G* level of theory, which means that the IET coordinate is very flat. Although at this level of computation the values of the barriers may not be exact, in principle our result agrees with experimental EPR data that indicate that the ground-state minimum of NRB has four equivalent olefinic hydrogens.[14] Due to the low IET barrier, the two localized species are in a dynamic equilibrium, and the hydrogens are equivalent. The low barrier is due to the proximity of the double bonds, which allows for a direct overlap of the π orbitals (mechanism iv).

The potential energy surface of PLN has an avoided crossing topology (type 1b). The avoided crossing can be seen as a limiting case of the sloped CI (type 1a) where the two states cross at infinity. The two low-lying states at the avoided crossing of C_{2v} symmetry are, in analogy to NRB, the $^2B_2$ ground state and the $^2A_1$ first excited state. In the optimized minimum **PLN-Loc** (Figure 5), the charge is localized in one of the π bonds. The C_{2v}-symmetry-restricted ground-state minimum ($^2B_2$) is **PLN-TS$_1$**. A frequency calculation shows that **PLN-TS$_1$** is the TS for IET between the two localized species, and the activation barrier is 0.6 kcal mol^{-1} (Figure 5). At **PLN-TS$_1$**, the two lowest states are separated by 6.8 kcal mol^{-1}, and the super-exchange IET occurs purely adiabatically (mechanism i). The calculated IET reaction coordinate (see Figure 6 and Computational Details) shows that the charge is transferred gradually along the coordinate, which is in agreement with the adiabatic character of the process. At **PLN-TS$_1$**, the gradient of the upper surface at that geometry is small (0.014 au). The geometry of the excited-state ($^2A_1$) minimum **PLN-EXC** is very similar to the one of **PLN-TS$_1$**, and no CI could be optimized for PLN, which shows that the crossing between the two states is always avoided.

The fact that the electronic $^2B_2$ and $^2A_1$ states of PLN are not degenerate at any geometry is an indication of the well-known fact that the charge-bearing double bonds are not isolated from one another, but rather interact through the norbornylogous

(14) Gerson, F.; Qin, X.-Z. *Helv. Chim. Acta* **1989**, *72*, 383−390.

Scheme 1

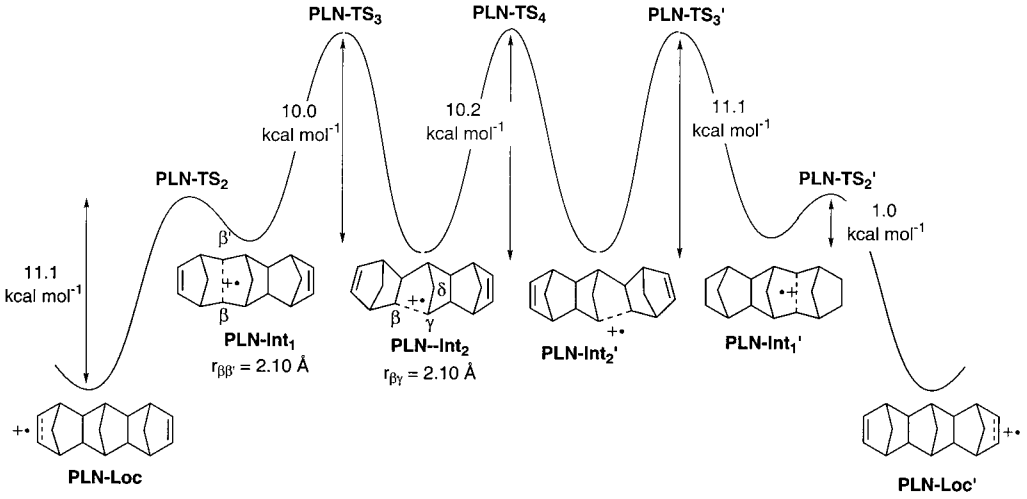

bridge.[6b] This interaction occurs by a through-bond coupling of the charge-bearing units through the σ orbitals of the bridge, and the magnitude of our calculated energy gap at the TS geometry is equivalent to the coupling term V of the MH model (see Figure 3). For PLN, this value has been estimated experimentally from the vertical π ionization split observed in photoelectron spectroscopy of the neutral compound.[8a,b] Our calculated energy gap of 6.8 kcal mol^{-1} (see Table 1) is in remarkably good agreement with the experimental ionization potential split of 7.4 kcal mol^{-1}. However, one should keep in mind that the latter estimate neglects the dependence of V on the geometry of the molecule. This is a reasonable assumption for PLN due to the small geometric changes associated to the ionization of the molecule and the IET coordinate, but it may not be correct for other systems.[15]

Although the through-bond coupling occurs through the σ orbitals of the bridge, the charge is not localized in these bonds at any time during this super-exchange mechanism (case i). On the contrary, the orbitals of the active space at **PLN-TS$_1$** are mainly localized in the π bonds. Although there is a small delocalization of the orbitals to the neighboring σ bonds, this occurs not only in the TS, but also at the localized minimum **PLN-Loc**. Therefore, the charge is actually not "migrating" through these bonds. Nevertheless, the "through-bond" interaction is responsible for the fact that the energy of the $^2B_2$ state is lower than the $^2A_1$ one, so that the two surfaces do not cross at any geometry. In fact, if the through-bond interaction is "switched off", the two states become degenerate. This was shown by a calculation on the radical cation of an ethylene dimer obtained by removing the alkyl bridge of PLN, and keeping the relative orientation and the bond lengths of the charge-bearing units in **PLN-TS$_1$**. In this case, where there is only through-space interaction and the distance between the ethylene monomers is 6.97 Å, the two low-lying states are virtually degenerate (separation 0.04 kcal mol^{-1}).

The different topologies calculated for NRB (type 1a, sloped CI) and PLN (type 1b, truly avoided crossing) can be understood as the result of the interplay between through-space and through-bond effects. In PLN, through-space interaction is negligible and the through-bond effect keeps the $^2B_2$ and the $^2A_1$ states apart at all geometries. However, in NRB the through-space and the through-bond interactions have opposite effects. Thus, natural bond orbital analyses carried out by Paddon-Row and co-workers[8b,c] have shown that the through-bond interaction in NRB destabilizes the A_1 orbital more than the B_2 one (in contrast to what occurs in PLN), while the through-space interaction stabilizes the A_1 orbital. At the geometry of **NRB−CI**, both effects cancel each other out and the states become degenerate.

Type 2 Topology: DAE. Type 2 topology was found for DAE. Here, two distinct IET mechanisms, the direct and a chemical one where the charge localizes in the ethylene linker (cases iv and iii, respectively), compete along different TS regions in the moat that surrounds a CI. We have studied the IET for the *gauche* configuration of the molecule, where the two amino groups lie on the same side of the carbon−carbon bond, and have not considered possible decomposition or isomerization paths. The optimized CI has C_{2v} symmetry (Figure 7b,d). At this symmetry, the two nitrogen atoms are equivalent, and the nonbonding orbitals lie in the plane of the molecule. The electronic states that cross at **DAE-CI** are $^2A_1$ and $^2B_2$ (Figure 7a). Two ground-state minima are found for the two states following the gradient difference from the CI in *opposite* directions. This gives rise to the moat topology (type 2) of the potential energy surface. The derivative coupling coordinate of b_2 symmetry is the antisymmetric stretching of the CN bonds (Figure 7b). This causes localization of the charge on one of the nitrogens and pyramidalization of the other, neutral one. This coordinate leads to a minimum of C_s symmetry (**DAE$_1$**, of $^2A'$ electronic state). In the full space of coordinates, **DAE$_1$** has a negative frequency that interconnects two equivalent conformers of the localized minimum **DAE-Loc** (Figure 7c). In this structure, there is a weak, stabilizing N−H bond between the lone pair of the neutral nitrogen atom and one of the hydrogen atoms of the charged nitrogen. This explains the charge localization, which does not occur in cyclic diamine analogues.[16]

The gradient difference coordinate at the intersection is a stretching of the carbon−carbon and nitrogen−nitrogen σ bonds. In the direction that shortens the bonds, the C_{2v} symmetry-restricted minimum of the $^2B_2$ electronic state, **DAE$_2$**, is found. **DAE$_2$** is a second-order saddle point, and one of its negative frequencies leads to a C_2 symmetry-restricted minimum of ^2B electronic state, **DAE-TS$_1$** (Figure 7e), which is a TS for the direct IET (Figure 2b). The N−N distance is 2.16 Å, and there is a direct overlap between the two orbital lobes. The activation barrier for this monorotatory process, in which the charge-

(15) Toutounji, M. M.; Ratner, M. A. *J. Phys. Chem. A* **2000**, *104*, 8566−8569.

(16) Brouwer, A. M.; Zwier, J. M.; Svendsen, C.; Mortensen, O. S.; Langkilde, F. W.; Wilbrandt, R. *J. Am. Chem. Soc.* **1998**, *120*, 3748−3757.

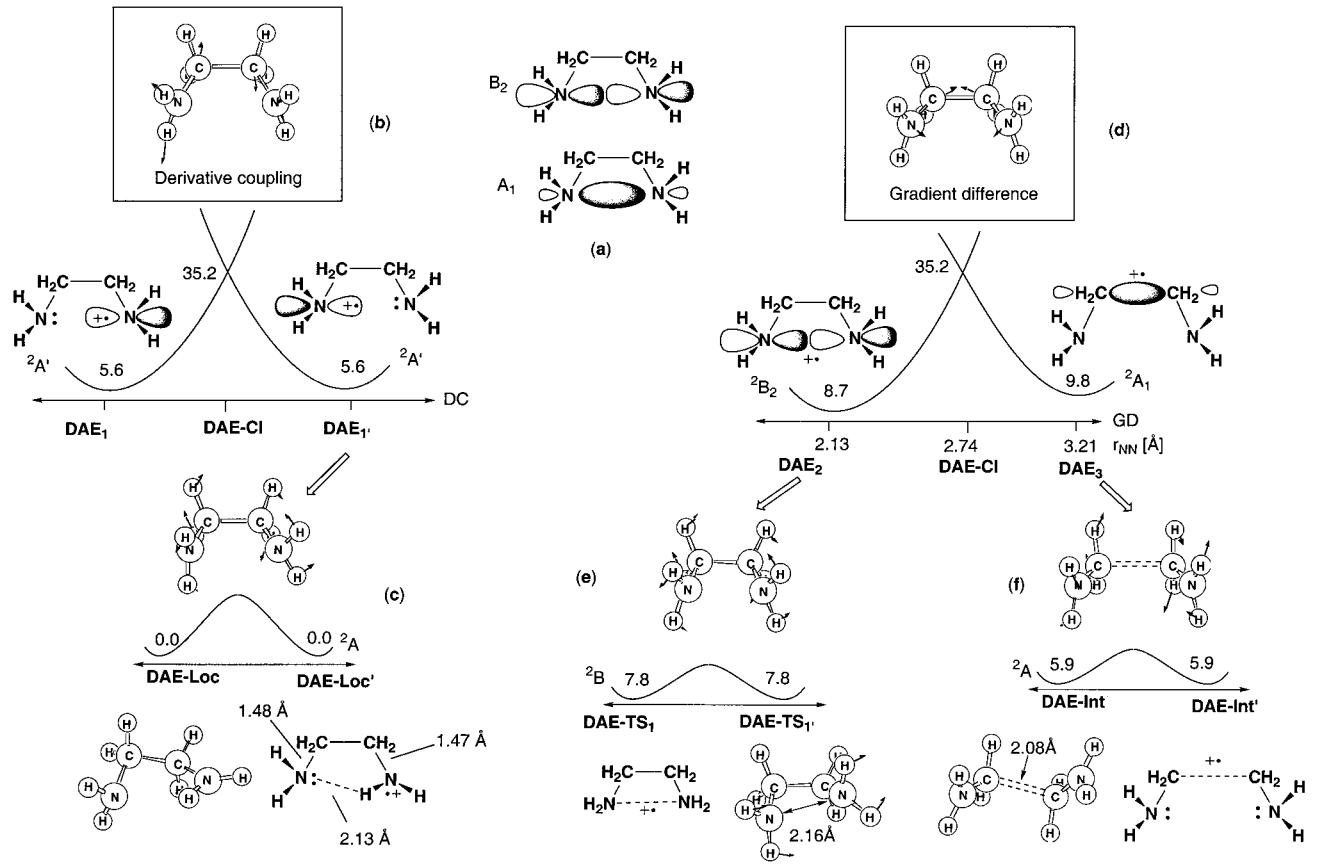

Figure 7. Branching of the EDA potential energy surface from the peaked CI along the derivative coupling (DC) and gradient difference (GD) coordinates (energies in kcal mol^{-1}).

bearing nitrogen rotates approximately 80° to reach the TS, is 7.8 kcal mol^{-1}. The height of the barrier is partly due to the energy required to break the weak N−H electron bond of the localized structure.

The minimum of the $^2A_1$ state was found stretching the C−C bond along the gradient difference coordinate that lengthens the C−C and N−N bonds. As the C−C bond is stretched, the N−N and the σ C−C orbitals, both of A_1 symmetry, mix. Thus, at the optimized geometry **DAE$_3$**, the charge is accommodated in the σ carbon−carbon bond, which is stretched to 2.20 Å. The two nitrogen atoms are neutral. The structure **DAE$_3$**, of C_{2v} symmetry, is a TS between two equivalent conformers **DAE-Int** of C_2 symmetry, which are minima in the full space of coordinates. **DAE-Int** is the intermediate for the CET path. In **DAE-Int**, the carbon−carbon σ bond is 2.08 Å long. **DAE-Int** lies 5.9 kcal mol^{-1} above the localized minimum **DAE-Loc** and is connected to it via **DAE-TS$_2$** (7.2 kcal mol^{-1} above **DAE-Loc**). The activation barriers for the CET path are 7.2 kcal mol^{-1} for the first step (**DAE-Loc** to **DAE-TS$_2$**), and 1.3 kcal mol^{-1} for the second step (**DAE-Int** to **DAE-TS$_2$**). Therefore, the chemical (7.2 kcal mol^{-1}) and the direct IET mechanisms (7.8 kcal mol^{-1}) for DAE have almost the same barrier, although the values may not be exact at the present level of theory.

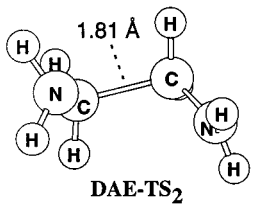

Clearly, both paths are adiabatic, since the relevant structures lie more than 20 kcal mol^{-1} below **DAE-CI** (see Table 1). Both cases will not adjust to a quantitative MH treatment, since there is direct orbital overlap between donor and acceptor (in the chemical mechanism, if each step is considered separately, the carbon−carbon σ bond becomes the donor viz. the acceptor).

Type 3 Topology: BMA. Type 3 topology, a seam of intersection, was found for the radical cation of bismethylene-adamantane (BMA). This molecule has a Jahn−Teller degeneracy of D_{2d} symmetry, and the degenerate orbitals are shown in Figure 8a. The minimum point of degeneracy was optimized as a CI. At **BMA-CI**, the charge is delocalized over the two double bonds. However, the Jahn−Teller minimum is not a stationary point of the potential energy surface (i.e., it has nonzero gradient), and therefore the D_{2d} structure is strictly not the TS for the IET. At **BMA-CI**, the derivative coupling coordinate (Figure 8b) is the asymmetric stretching of the double bonds that causes charge localization. The localized minimum **BMA-Loc**, of C_{2v} symmetry, lies 3.4 kcal mol^{-1} below the intersection. This point was optimized and characterized by a frequency calculation at the CAS(3,4)/3-21G* level. The frequency calculation showed one low imaginary frequency (135*i* cm^{-1}), corresponding to the pyramidalization of the methylene group of the charge-bearing unit. However, we were not able to optimize any minimum of lower symmetry (C_s or C_1). This means that the potential energy surface around **BMA-Loc** is flat. It may also be sensitive to the level of theory, as can be inferred from the low value of the imaginary frequency. At the AM1-CI level of theory, the one-electron π bond of the localized BMA minimum is twisted by 22.5° away from the C_{2v} conformation, and this is supported by experimental and computational findings on ethylene radical cation.[9] Certainly

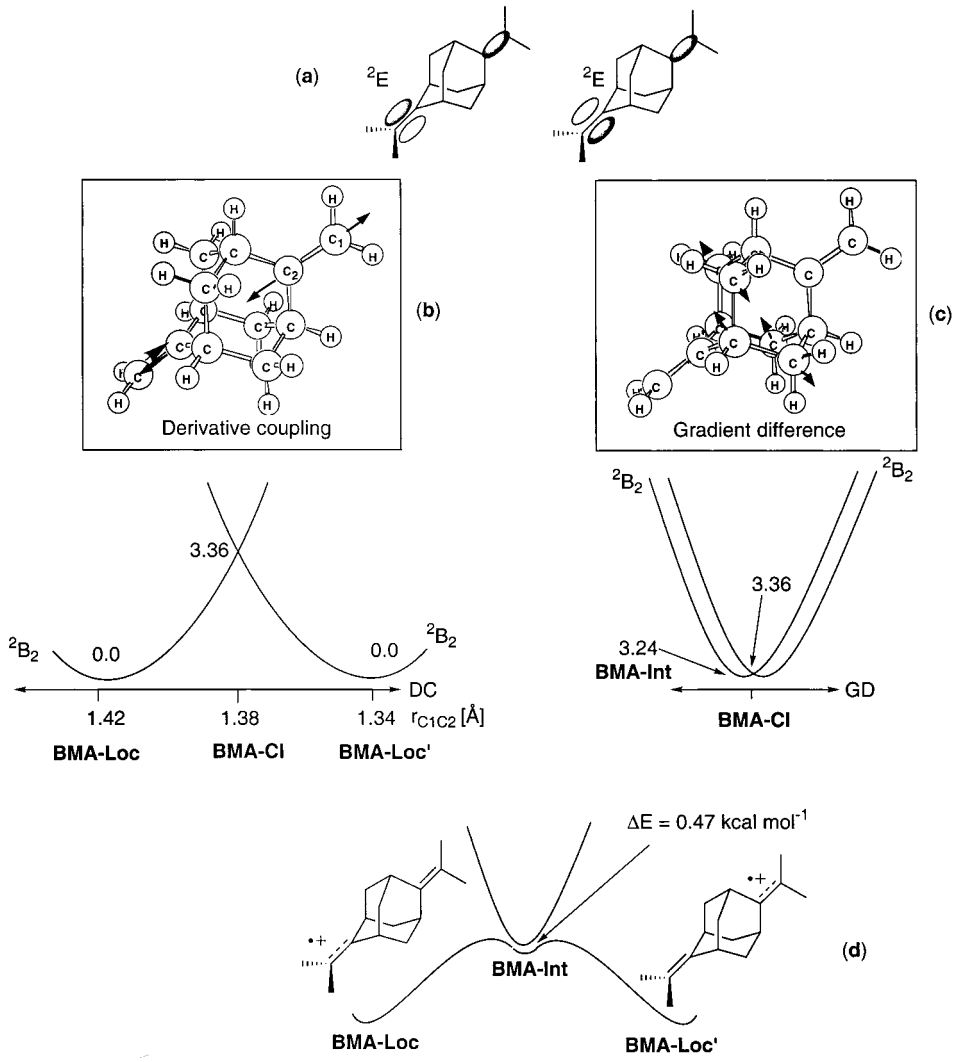

Figure 8. Branching of the BMA Jahn−Teller potential energy surface along the derivative coupling (DC) and gradient difference (GD) coordinates (energies in kcal mol^{-1}).

this point should be clarified by future higher-level calculations, but since we are interested in the topology of the potential energy surface around the state crossing rather than at the minimum geometry, it should not affect our conclusions on the seam topology found for BMA.

At **BMA-CI**, the length of the gradient difference vector is very small (0.0098 au), which indicates that we have effectively the seam topology corresponding to type 3 (the gradient difference vector will never have zero length identically, it can only become vanishingly small). A very small distortion along the gradient difference coordinate in opposite directions leads to very shallow equivalent minima **BMA-Int** of D_2 symmetry, only 0.12 kcal mol^{-1} lower in energy than the CI. At **BMA-Int**, the energy difference between ground and excited state is only 0.47 kcal mol^{-1}. Thus the minima of D_2 symmetry are virtually coincident with the Jahn−Teller degeneracy. An analytical frequency calculation showed that **BMA-Int** is a minimum in the full space of coordinates. The IET reaction coordinate was estimated by a series of single-point calculations on structures obtained by linear interpolation (see Figure S1, Supporting Information). A continuous energy decrease from **BMA-Int** to **BMA-Loc** was obtained, which indicates that **BMA-Int** is a shallow minimum on the potential energy surface and the TS region is flat. Carpenter and Paddon-Row suggest (as a result of AM1-CI computations) that the IET in BMA is "symmetry-forbidden",[9] since the super-exchange coupling vanishes due to the orientation of the double bonds toward each other. In effect, the IET will be completely nonadiabatic (case ii), because the energy separation at **BMA-TS** (0.02 eV) is smaller than the value of 0.025 eV given as limit for adiabatic regime.[17] Therefore, this Jahn−Teller degeneracy can be classified as a seam (type 3) of intersection.[2b]

The nonadiabatic nature of the process is also reflected in the charge-transfer coordinate given in Figure 6 (see Computational Details). In sharp contrast to the gradual IET found for PLN, virtually no charge transfer is detected along the IET coordinate for BMA until the molecule reaches the TS, where the charge, from a formal point of view, is transferred "instantaneously". AM1-CI dynamics calculations[9] suggest that symmetry-breaking distortions of the methylene groups may be the origin of avoided crossing paths for the adiabatic (i.e., allowed) charge transfer. This idea can only be tested by further dynamics studies at a higher, more reliable level which will be necessary to understand the mechanism of this model NAET.

CET for PLN. In the competing chemical mechanism for PLN, the charge migrates stepwise, localizing on the carbon−carbon bonds of the bridge (see Scheme 1). A topology of type 2 (peaked CI) has been found for the first step of the chemical mechanism (see Figure 9). We have optimized two intermediates, **PLN−Int$_1$** and **PLN−Int$_2$**, where the charge is accom-

(17) Farazdel, A.; Dupuis, M.; Clementi, E.; Aviram, A. *J. Am. Chem. Soc.* **1990**, *112*, 4206.

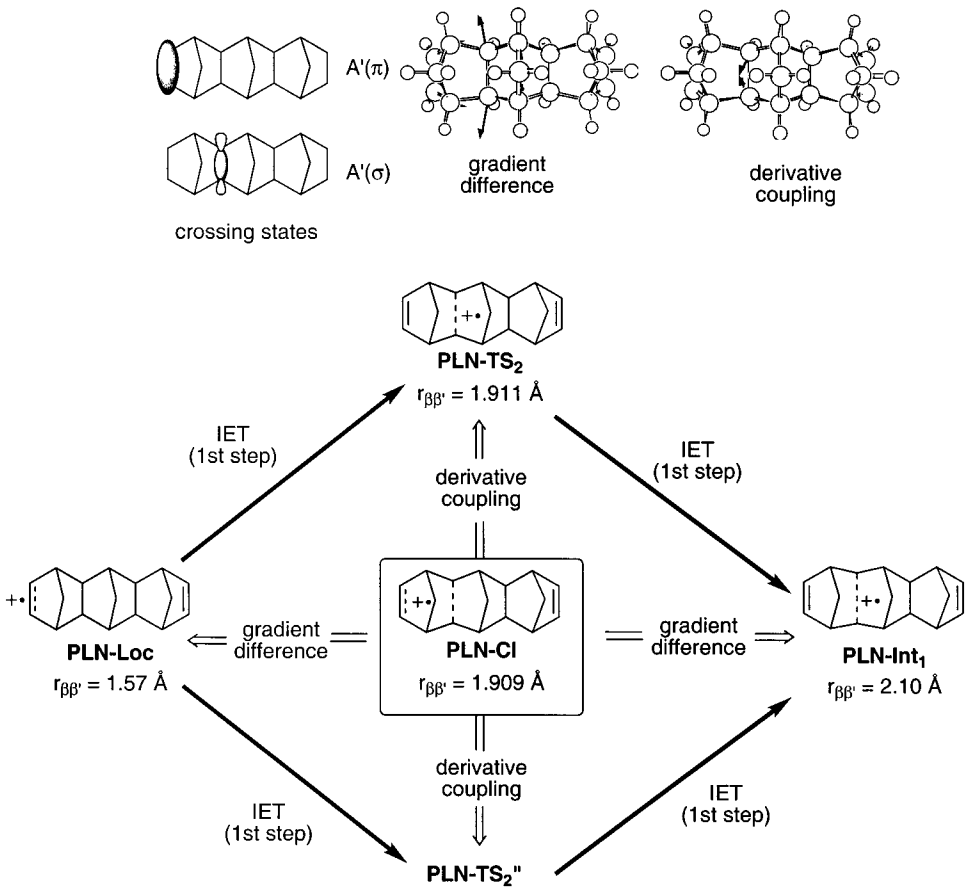

Figure 9. Schematic representation of the moat topology for the CI between the σ and π states of PLN (first step of the chemical mechanism).

modated in the $\beta\beta'$ and the $\beta\gamma$ carbon−carbon σ bonds, respectively. These bonds are stretched to 2.10 Å. Further, we have optimized the TSs that connect the localized minima and the intermediates. This completes the CET path, of 5 steps.

The path is adiabatic (case iii), because the separation between the states is larger than 10 kcal mol^{-1} for all structures involved (see Table 1). It is clear from Scheme 1 that the chemical path requires higher activation barriers (approximately 10 kcal mol^{-1} for each step) than the super-exchange path (0.6 kcal mol^{-1}) documented in the preceding discussion of a type 1 surface topology. Moreover, the efficiency of the stepwise path is reduced by the high degree of reversibility for the first step, since the barrier for the reverse step from **PLN**−**Int$_1$** to **PLN-Loc** is only 1.0 kcal mol^{-1}. Even if the first step of the stepwise path may be accomplished, the reaction will go "back" to the π-localized structure rather than go "further" to the next σ-localized one. In conclusion, the stepwise CET is not relevant for PLN, but a σ-localized intermediate has been suggested for IET in a PLN analogue on the basis of dynamics calculations.[8d] There, the alkyl bridge contained two fused cyclobutyl rings with a highly strained σ bond where the charge could localize. Our calculations show that such an intermediate is possible, although we cannot assess the energetics of its chemical path here.

The first step of the chemical mechanism for PLN illustrates our type 2 (Figure 2) model for ET in the moat of a conical intersection. In this case, the charge is transferred from one of the terminal π bonds to the $\beta\beta'$ carbon−carbon σ bond. The IET takes place between two nonequivalent structures. (The gradient difference and derivative coupling vectors are reversed from the previous discussions because the states involved at the conical intersection are quasi-localized. Thus, the IET reaction path coincides with the gradient difference vector, see Theoretical Considerations). Consistent with the type 2 topology, there is a peaked conical intersection, **PLN**−**CI**, between both states. The topology around **PLN**−**CI** is similar to that of the moat shown for DAE radical cation in Figure 2b and is presented schematically in Figure 9. The adiabatic IET path between the two charge localized minima is via the avoided crossing that goes through **PLN-TS$_2$** (found along the derivative coupling coordinate from the CI), in the moat of the conical intersection. One would expect the existence of two different paths along either side of the moat, as we have shown in our bis(hydrazine) study[2b] and for DAE. However, the potential energy surface along the derivative coupling is shallow, as seen by the proximity of the TS to the CI, and only one TS could be found.

Conclusions

The potential energy surface topology for IET in organic radical cations can be classified into three types (Figure 2) according to the shape of the state-crossing region (in the space of the degeneracy-lifting coordinates of a conical intersection). In this paper we have shown how these topologies can arise in some "model" chemical systems. The three types of mechanistic topology cover all possibilities for IET transition state regions. The different topologies can coexist and, in principle, compete on different regions of the potential energy surface of the same molecule, giving a more diverse mechanistic description than the usual MH analysis, which is limited to one reaction coordinate.

Our calculated topologies can be related to the four possible IET mechanisms (super-exchange, nonadiabatic, chemical, and direct). The super-exchange mechanism (case i) in PLN is associated to a truly avoided crossing (type 1b). This result can

be expected to be general, since the super-exchange interaction will keep the two low-lying states apart and prevent the crossing. Clearly, the NAET mechanism (case ii) corresponds to a seam of intersection (type 3 topology), as seen here for BMA and in a previous example for a bis(hydrazine) radical cation.[2b] Finally, the chemical and direct mechanisms (cases iii and iv) are associated to a peaked CI (type 2) for DAE and the PLN chemical path (see also the chemical mechanism for IET in a bis(hydrazine) model[2b]), and to a sloped CI (type 1a) for the direct mechanism in NRB. At the present stage, this classification is only approximate and has to be refined by further examples.

Finally, our results highlight the role of alkyl linkers in IET. We have optimized chemical paths, alternative to the super-exchange and direct mechanisms, which go through intermediates where the charge is localized on the carbon−carbon σ bonds of the linker. In DAE, the CET path is slightly preferred over the competing direct path. In PLN, the super-exchange path is clearly the lowest-energy one. Here, the rigid alkyl bridge lowers the IET barrier providing through-bond interaction between the two charge-bearing groups. However, the charge never actually migrates through the σ bonds, and the spacer remains neutral during the IET. The path where the bridge gets charged corresponds to the chemical mechanism, which has higher barriers and is less efficient.

Acknowledgment. All computations were carried out on an IBM-SP2 funded jointly by IBM-UK and HEFCE (UK). We are grateful to the European Community for a Marie Curie Fellowship to L. B. (Grant No. ERB4001GT964926) and to F. J. (Grant No. ERBFMBICT97828). The collaboration between M.A.R. and M.O. is financed by a Nato Grant CRG 950748.

Supporting Information Available: Absolute energies and active spaces for all structures reported (Tables S1-S3); Cartesian coordinates of all structures; and linearly interpolated reaction coordinate between **BMA-Loc** and **BMA-Int** (Figure S1) (PDF). This material is avaiable free of charge via the Internet at http://pubs.acs.org.

JA003359W